4. RESULTS AND DISCUSSION

4.1. V_2O_3 - TiO_2 System

Table 4.1. gives a summary of the sample compositions reacted, the reaction times used and phases identified in each sample. All of the samples were subjected to XRD analysis, optical microscopy under reflected light and EPMA, with WDS and EDS facilities respectively.

Table 4.1: Summary of Experiments

Reaction Temperature (°C)	Initial Composition (Mass %)		Reaction Time (Hours)	Phases Identified	mol Ti/ (mol Ti +mol V) in Phase
	TiO_2	V_2O_5			
1400	10	90	24	M_2O_3	$M_2O_3 = 0.08$
1400	30	70	24	$M_2O_3 + M_3O_5$	$M_2O_3 = 0.21$ $M_3O_5 = 0.35$
1400	50	50	24	$M_3O_5 + M_4O_7$	$M_3O_5 = 0.64$ M_4O_7 = N.A.
1400	70	30	24	Magneli	Magneli = 0.72
1400	90	10	24	Magneli	Magneli = 0.91
1500	10	90	24	M_2O_3	$M_2O_3 = 0.15$
1500	30	70	24	$M_2O_3 + M_3O_5$	$M_2O_3 = 0.17$ $M_3O_5 = 0.40$
1500	50	50	24	$M_3O_5 + M_4O_7$	$M_3O_5 = 0.42$ $M_4O_7 = 0.55$
1500	70	30	24	Magneli	Magneli = 0.73
1500	90	10	24	Magneli	Magneli = 0.91
1600	90	10	8	Magneli	Magneli = 0.91

The pseudo-binary V_2O_3-TiO_2 phase diagram constructed from the experimental data is shown in Fig. 4.1, and a summary of the EPMA analyses is given in Appendix 3 and Appendix 4. The phase fields identified are M_2O_3, $M_2O_3 + M_3O_5$ and Magneli phases, with M designating both vanadium and titanium ions existing within the particular crystal structure. As mentioned earlier, Magneli phases are crystallographic shear structures represented by the general formula Ti_nO_{2n-1} for Ti-O mixtures.[21] The phases with $4 \leq n \leq 10$ have crystal structures derived from the rutile structure.[12] Phases with $n > 10$ have structures based on other shear planes and so form different families of phases.[21] Both vanadium and titanium oxides form Magneli phases.[21,19]

The XRD patterns for the series of samples reacted at 1400°C are shown in Fig. 4.4. The corresponding photomicrographs for the samples are shown in Fig. 4.5. In Table 4.2 the

number of moles of Ti and V in the initial sample and in the reacted sample, for the single phase samples, are indicated. In the experiments only oxygen should have been removed from the sample because of reaction of the sample under reducing conditions with respect to the initial sample composition. Therefore the ratio of the number of moles of Ti to the number of moles of V in the initial sample should correspond with that of the reacted sample, as is the case in Table 4.2.

The 10 mass% TiO_2 sample consisted of the M_2O_3 phase only indicated by the composition points 0.08 mole fraction Ti at 1400°C and 0.15 mole fraction Ti at 1500°C in Fig. 4.1. The 30 mass% TiO_2 sample consisted of the M_2O_3 phase and M_3O_5 phase which are clearly identified by the XRD analyses shown in Fig. 4.4. The two respective phases could only be distinguished from each other under reflected light when large magnifications were employed, i.e. x400 and larger. The M_2O_3 phase appear pink, and the M_2O_5 phase yellow under reflected light. The M_2O_3 phase appeared as the lighter grey phase, and the M_3O_5 phase as the darker grey phase when viewed with the SEM-EDS facility.

The EPMA (EDS) analyses for the TiO_2-V_2O_3 samples were checked by performing analyses with an ARL-SEMQ (WDS)-Wave Dispersive Spectrometer, employing VO_2 and TiO_2 physical standards. Good agreement was obtained as is seen when the EPMA (EDS) analyses in Appendix 4 are compared to the EPMA (WDS) analyses in Appendix 3. For all of the single phase samples the agreement between the EPMA analyses done with the WDS facility and those done with the EDS facility is excellent. The WDS analyses were used to plot composition points on the phase diagram in Fig. 4.1 for the samples consisting of a single phase.

For the samples consisting of two phases, differences between the two sets of analyses do occur because one of the phases was not analysed with either one of the facilities. Due to the limited optical capability of the WDS facility phases could not be distinguished visually from each other. This resulted in different proportions of each phase being analysed, on each point chosen for analysis, resulting in a distribution of analyses. Therefore a frequency distribution was constructed for the analyses done on the samples as is shown in Fig. 4.2 and Fig. 4.3 for the 30T14 and 50T15 samples.

Subsequently the data were divided into two groups with the division point for the 30T14 sample being 26 mass% TiO_2 and that for the 50T15 sample 50 mass% TiO_2. The division

point for the 30T14 sample was decided with reference to the EDS analyses already in hand. For the 50T15 sample the division point was taken according to the obvious data grouping as shown in Fig. 4.3 because only one phase was analysed with the EDS facility. The respective groups of data were subjected to Chauvenet's criterion[26] in order to eliminate data points deviating significantly from the normal distribution. The remaining data points were used to plot Fig. 4.1.

For the 30T15* and 50T14 samples only one of the two phases present in the sample was analysed by the WDS facility. The WDS analysis data for these samples were also subjected to Chauvenet's criterion[26]. For the 50T14 sample the remaining data were then used to plot the composition point for only the M_4O_7 Magneli phase in Fig. 4.1. For the 30T15 sample the remaining data were combined with the EDS facility's data because it is evident from the EDS data and the XRD analysis that one of the two phases in the sample was not analysed with the WDS facility due to the operator not being able to distinguish between the two phases whilst with the EDS facility one could clearly distinguish between the phases.

*Code clarification: The first two numbers and the following letter together indicate the initial sample composition, the next two code digits indicate the temperature at which the sample was reacted. If more digits follow they indicate the reaction time in minutes. If no digits follow to indicate the reaction time the reaction time was 24 hours. Therefore the 30T14 code means that the sample with the initial composition of 30 mass% TiO_2-70 mass% V_2O_5 (the 70 mass% V_2O_5 is implied because only TiO_2-V_2O_5 and Fe_2O_3-V_2O_5 mixtures were reacted); was reacted at 1400°C for 24 hours. F indicates Fe_2O_3 in the Fe_2O_3-V_2O_5 samples.

Fig. 4.1: V_2O_3 - TiO_2 Phase Diagram

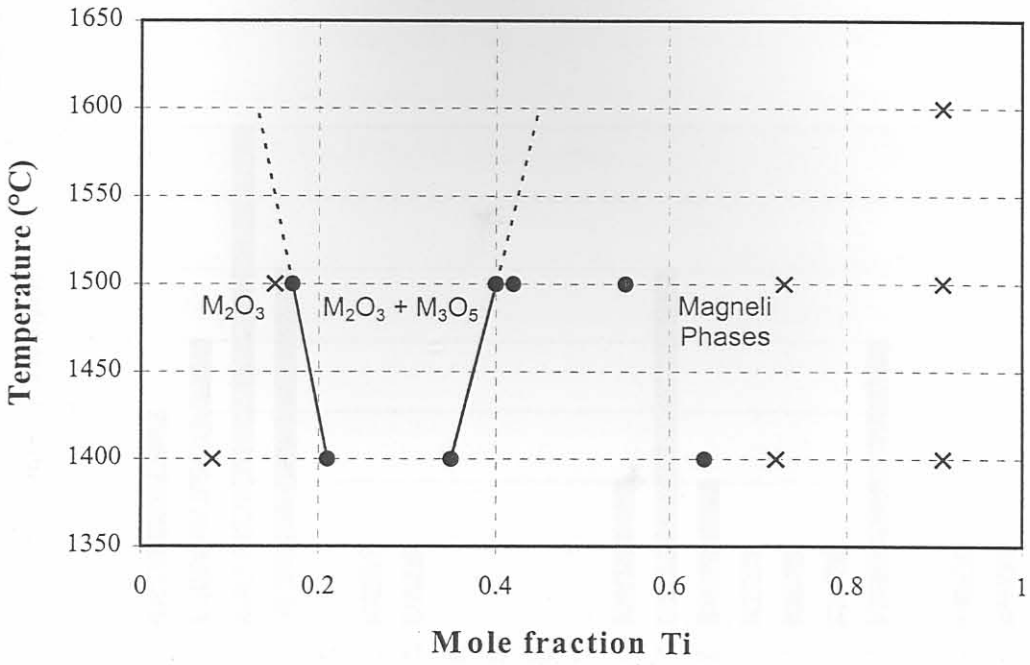

× : Composition points of samples consisting of one phase

• : Composition points of respective phases in two phase samples

Fig. 4.2: Analyses Frequency Distribution for 30T14 Sample (WDS analyses)

(XRD data indicate the presence of M_2O_3 and M_3O_5 phases-see Table 4.1)

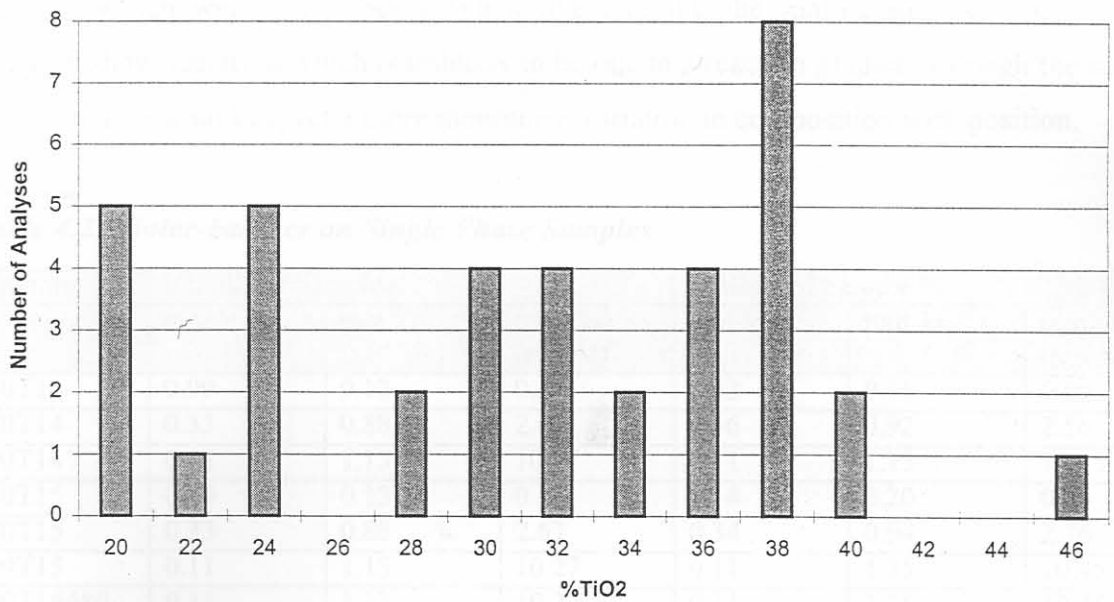

Fig. 4.3: Analyses Frequency Distribution for 50T15 Sample (WDS analyses)

(XRD data indicate the presence of M_3O_5 and M_4O_7 phases-see Table 4.1)

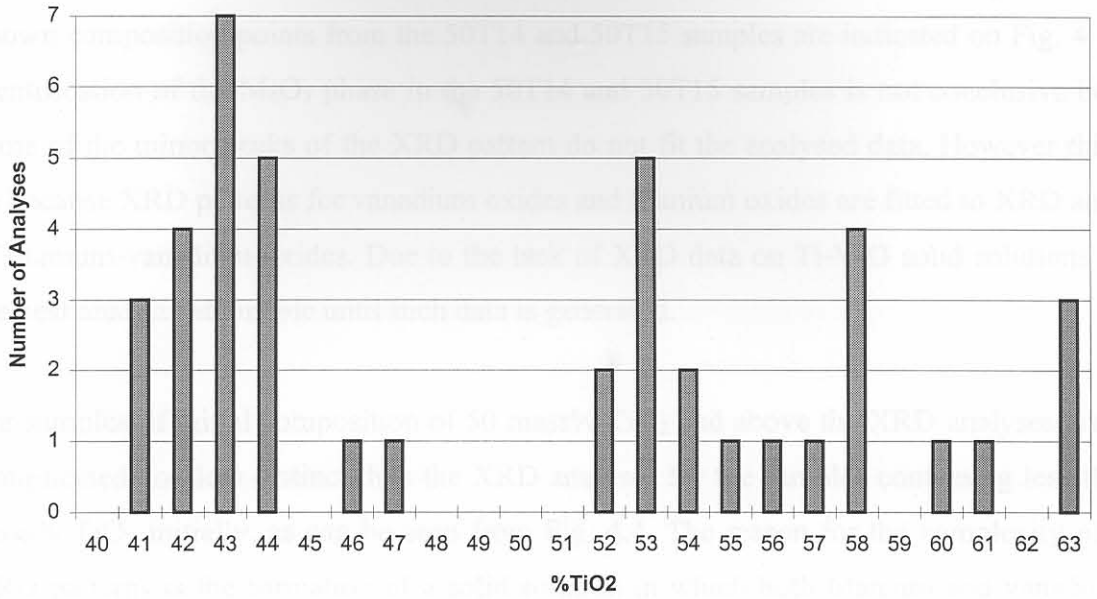

The 30T14, 30T15, 50T14 and 50T15 samples each contains two phases as indicated by the XRD analyses. In the 30T14 and 30T15 samples the respective phases could also be seen under reflected light and under the SEM(EDS). However, for the 50T14 and 50T15 samples the respective phases in each sample could only be identified with XRD analysis. The presence of two different phases in the 50T15 sample is supported by the EPMA(WDS) point analyses which were performed along a line crossing the sample surface, Fig. 4.7. The analyses show variation which is unlikely to be due to a reaction gradient through the sample, for which one would expect a more monotonic variation in composition with position.

Table 4.2: Molar-balance on Single Phase Samples

Sample	Initially in Sample			In Reacted Sample		
	mol V	mol Ti	(mol Ti)/ (mol V)	mol V	mol Ti	(mol Ti)/ (mol V)
10T14	0.99	0.13	0.13	1.22	0.11	0.09
70T14	0.33	0.88	2.67	0.36	0.92	2.56
90T14	0.11	1.13	10.27	0.11	1.15	10.45
10T15	0.99	0.13	0.13	1.14	0.20	0.18
70T15	0.33	0.88	2.67	0.34	0.94	2.76
90T15	0.11	1.13	10.27	0.11	1.15	10.45
90T16480	0.11	1.13	10.27	0.11	1.15	10.45

Due to the inability to distinguish the phases from each other when using the WDS facility only one of the phases was analysed in the 50T14 sample. The EDS analyses on the 50T14 and 50T15 samples were few and varied and not deemed conclusive. Therefore the phase boundary between the M_3O_5 and M_4O_7 phases could not be plotted onto Fig. 4.1, but the known composition points from the 50T14 and 50T15 samples are indicated on Fig. 4.1. The identification of the M_4O_7 phase in the 50T14 and 50T15 samples is not conclusive because some of the minor peaks of the XRD pattern do not fit the analysed data. However this may be because XRD patterns for vanadium oxides and titanium oxides are fitted to XRD analyses of titanium-vanadium-oxides. Due to the lack of XRD data on Ti-V-O solid solutions this is the best analysis attainable until such data is generated.

For samples of initial composition of 50 mass% TiO_2 and above the XRD analyses are more complicated and less distinct than the XRD analyses for the samples containing less than 50 mass% TiO_2 initially, as can be seen from Fig. 4.4. The reason for the complexity of these XRD patterns is the formation of a solid solution in which both titanium and vanadium are present. The XRD pattern will be further complicated by the presence of two solid solution phases in each sample. Although XRD data exist for the Ti_nO_{2n-1} ($4 \leq n \leq 10$) and V_nO_{2n-1} ($4 \leq n \leq 8$) Magneli phases, little XRD data could be found for the solid solution compositions of the type $(Ti, V)_nO_{2n-1}$. The available data are for the components $V_3Ti_6O_{17}$, $V_2Ti_7O_{17}$, $V_2Ti_3O_9$ and V_2TiO_5. For the 70T14 and 70T15 samples the XRD patterns of V_5O_9, V_7O_{13}, Ti_5O_9 and Ti_6O_{11} fitted the XRD analyses data the best. This is shown in Fig. 4.8. Even though these patterns fit the XRD analyses there remain unassigned peaks in the XRD analyses. This could perhaps be due to the XRD reference data not yet being determined at higher values of θ, or due to a more complicated XRD pattern formed because of both vanadium and titanium contained in the crystal structure, instead of just vanadium or titanium.

For the 90T14, 90T15 and 90T16480 samples none of the titanium oxide XRD patterns, or the vanadium oxide patterns fitted the XRD analyses, not even closely. The best fit was attained for the $V_2Ti_7O_{17}$ XRD pattern, but only filling some of the peaks in the XRD analyses data. Because the XRD patterns corresponding most favourably with the experimental data of the samples with $\geq$ 50 mass% TiO_2, initial sample composition, were those of the Magneli phases with the general formula of M_nO_{2n-1}, the phase diagram in Fig. 4.1. has the phase field between M_3O_5 and TiO_2 designated as Magneli phases. The existence of M_nO_{2n-1} with n=6,7,8,9,10 was found by Kosuge and Kachi[27] in the TiO_2-V_2O_3 pseudo-binary system

within the high TiO_2 compositional area, supporting the designation of phases within the high TiO_2 side of the TiO_2-V_2O_3 pseudo-binary diagram in Fig. 4.1 as Magneli phases.

Zador and Alcock[20] determined the partial oxygen pressure stability ranges for titanium containing Magneli phases at 1300°C, 1400°C and 1500°C. The data at 1400°C and 1500°C is summarised in Table 4.3. The partial oxygen pressures employed by Zador and Alcock[20] are more reducing than those employed in the present study, that is 3.02×10^{-10} atm at 1400°C and 2.99×10^{-9} atm at 1500°C. According to Zador and Alcock's data one would expect a pure TiO_2 sample reacted at these temperatures and partial oxygen pressures to have a rutile structure. This is confirmed by a sample reacted in the present study at 1500°C, under a partial oxygen pressure of 1.26×10^{-9} atm, for 18 hours. The XRD pattern for the sample is shown in Fig. 4.6 and it can be seen that the pattern for rutile fits. Therefore it appears that the Magneli phases in the high TiO_2 samples (≥ 50 mass% TiO_2 in initial sample) are stabilised by the vanadium additions.

In Table 4.4 the ionic radii for titanium and vanadium cations are compared. If the difference in ionic radii is in excess of 15%, substitutional solid solution formation is unlikely.[25] Therefore, with reference to Table 4.4., V^{5+}, V^{4+} and V^{3+} can substitute for Ti^{4+} and V^{2+} and V^{3+} can substitute for Ti^{3+}.

Table 4.3: Partial Oxygen Pressure Stability Ranges for Magneli Phases at 1400°C and 1500°C *(Zador and Alcock[20])*

Components	P_{O_2} (atm)	
	1400°C	1500°C
Ti_3O_5-Ti_4O_7	8.40×10^{-14}	2.24×10^{-12}
Ti_4O_7-Ti_5O_9	1.24×10^{-13}	----------
Ti_5O_9-Ti_6O_{11}	4.14×10^{-13}	6.09×10^{-12}
Ti_6O_{11}-Ti_7O_{13}	7.53×10^{-13}	1.01×10^{-11}
Ti_7O_{13}-Ti_8O_{15}	9.61×10^{-13}	----------
Ti_8O_{15}-Ti_9O_{17}	1.30×10^{-12}	1.64×10^{-11}
Ti_9O_{17}-$Ti_{10}O_{19}$	1.50×10^{-12}	1.99×10^{-11}
$Ti_{10}O_{19}$-$Ti_{20}O_{39}$	1.92×10^{-12}	2.80×10^{-11}
$Ti_{20}O_{39}$-TiO_2	4.71×10^{-12}	1.42×10^{-10}

Similarly, the binary system Cr_2O_3-TiO_2 contains a series of shear phases $Ti_{n-2}Cr_2O_{2n-1}$, n = 6 to 11, in which the oxygen-to-metal ratio is reduced by substitution of Cr^{3+} for Ti^{4+}.[27] Vanadium and chromium are both transition elements on the periodic table, and are situated next to each other on the periodic table, indicating that the chemical behaviour of these two

elements is similar. Therefore the behaviour of V in the TiO_2-V_2O_3 system should be similar to that of Cr in the TiO_2-Cr_2O_3 system. However, accordingly to Table 4.4 one expect V^{4+} to substitute for Ti^{4+}, and V^{3+} to substitute for Ti^{3+}.

According to Handfield and Charette[28] the structure of molten high TiO_2 slags should be similar to that of the corresponding solid slags since the electrical properties of these slags changed very little in passing from solid to the liquid state. Thus the solid solution formation of mixtures of TiO_2 and V_2O_3, in Magneli phase co-ordination, found in this work should prevail when these mixtures are melted.

According to Reznichenko et al.,[29,30] as discussed by Handfield and Charette,[28] high titania slags in the solid state consist of a solid solution based on the Ti_3O_5 type structure (orthorhombic), and a solid solution of the Ti_2O_3 type structure (rhombohedral) and glassy materials filling the spaces between the crystals. Depending on the slag composition any one of the solid solutions can form. The proposed general formula for the respective solid solutions are: for the Ti_3O_5 solid solution: m[(Ti, Mg, Mn, Fe)O.2TiO_2]•n[(Ti, Fe, Al, Cr, V)$_2O_3$.TiO_2]; for the Ti_2O_3 solid solution: a[(Ti, Mg, Mn, Fe)O.TiO_2]•b[(Ti, Fe, Al, Cr, V)$_2O_3$]. According to the above vanadium and chromium exist as V^{3+} and Cr^{3+}, and iron as Fe^{2+} and Fe^{3+} within these high TiO_2 solids and slags.

Table 4.4: Radii of Cations[24]

Cation	Radius (Å)	%Difference with respect to Ti^{4+} radius = 0.68 Å	%Difference with respect to Ti^{3+} radius = 0.76 Å
V^{5+}	0.59	13	22
V^{4+}	0.63	7	17
V^{3+}	0.74	8	2.6
V^{2+}	0.88	22	14

Fig. 4.4: XRD Patterns for TiO_2 - V_2O_5 Samples reacted at 1400°C

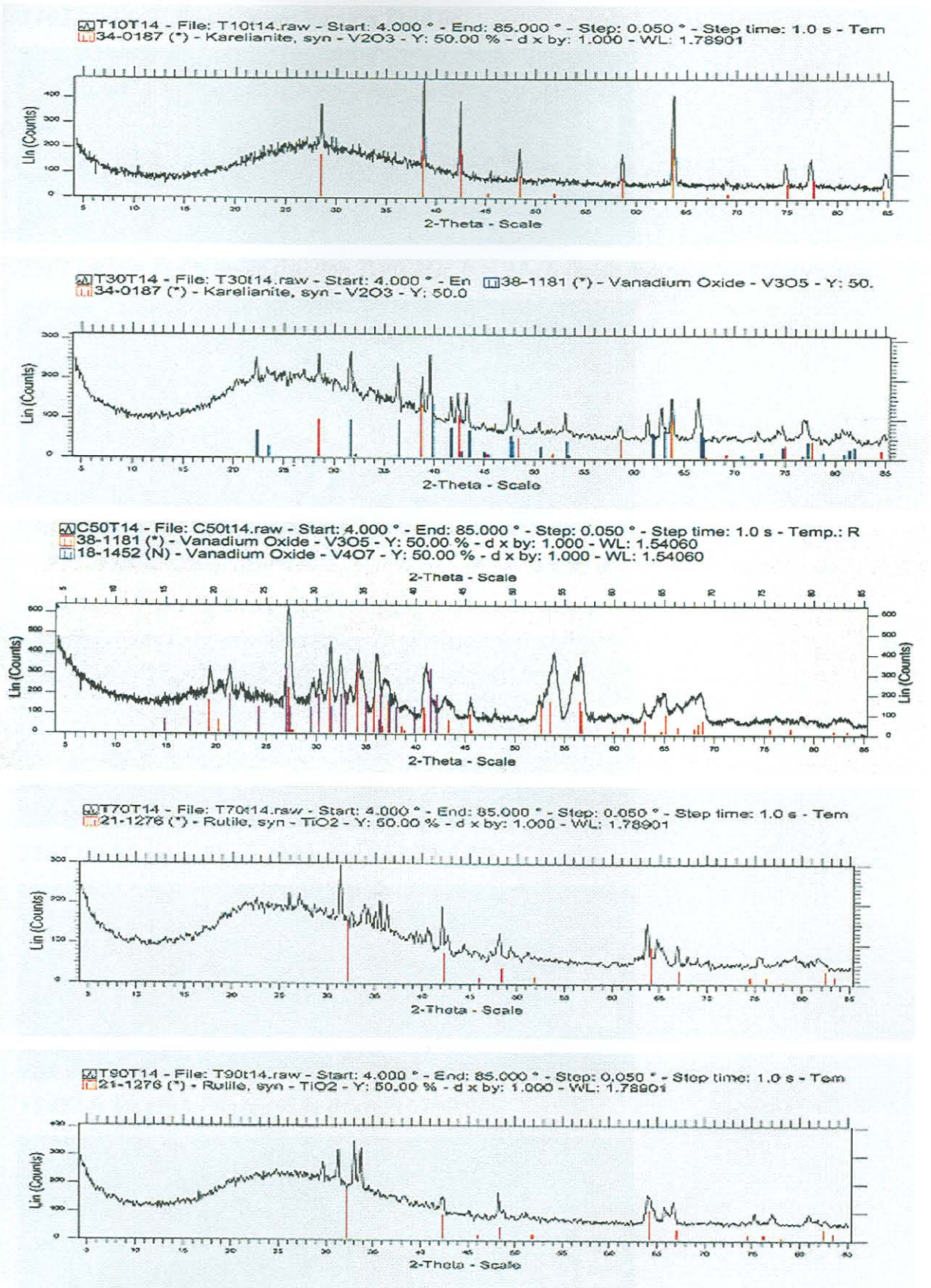

T10T14 = 10 mass% TiO_2 in initial sample; T30T14 = 30 mass% TiO_2 in initial sample;

T50T14 = 50 mass% TiO_2 in initial sample; T70T14 = 70 mass% TiO_2 in initial sample;

T90T14 = 90 mass% TiO_2 in initial sample

Fig. 4.5: Photomicrographs for TiO_2 - V_2O_5 Samples reacted at 1400°C

T10T14: *M_2O_3 Phase (mole fraction Ti=0.08)*

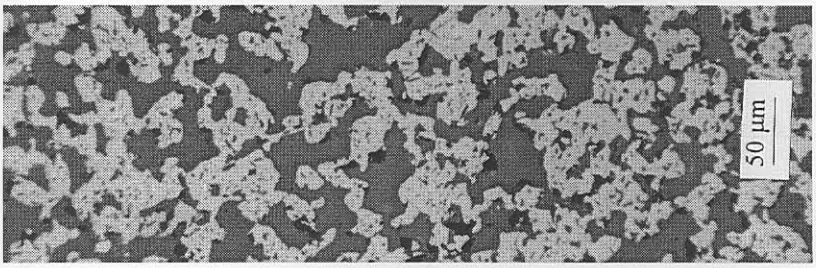

T30T14: *a = M_2O_3 (mole fraction Ti=0.21); b = M_3O_5 (mole fraction Ti=0.35);(x400)*

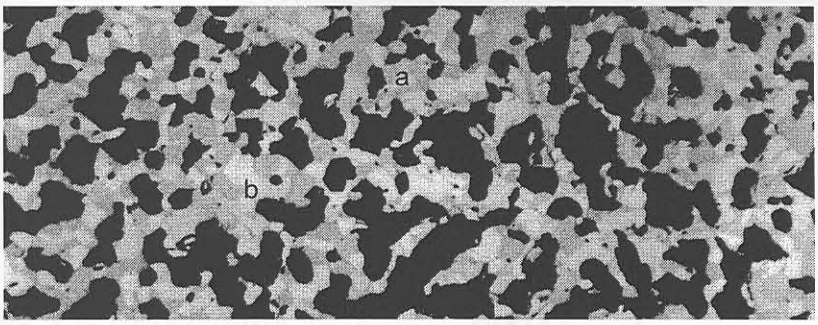

T50T14: *(M_3O_5(mole fraction Ti=0.64) and M_4O_7 according to XRD analysis, but only one phase seen under reflected light at magnifications employed)*

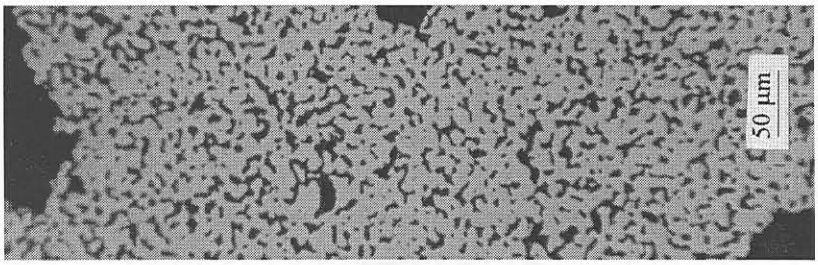

T70T14: *Magneli Phase (mole fraction Ti=0.72)*

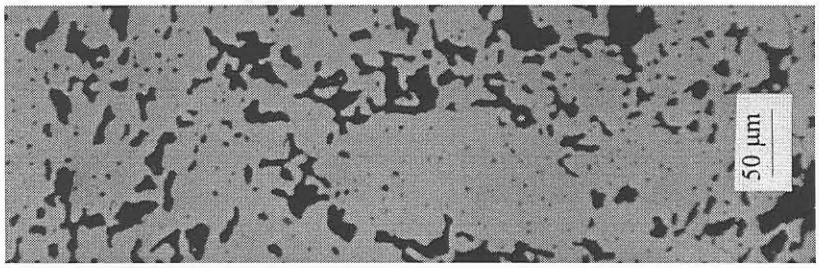

T90T14: *Magneli Phase (mole fraction Ti=0.91)*

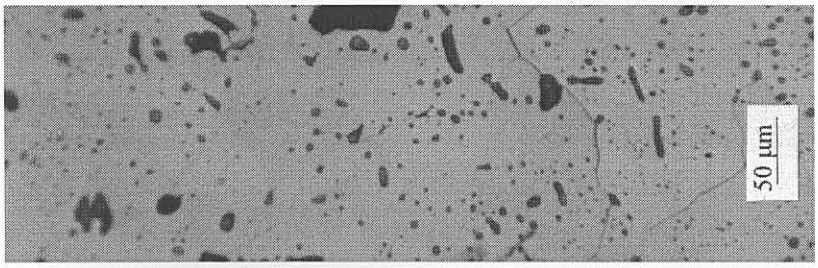

T10T14 = 10 mass% TiO_2 in initial sample; T30T14 = 30 mass% TiO_2 in initial sample;
T50T14 = 50 mass% TiO_2 in initial sample; T70T14 = 70 mass% TiO_2 in initial sample;
T90T14 = 90 mass% TiO_2 in initial sample

Fig. 4.6: XRD Pattern for 100% TiO_2 Sample Reacted for 18 hours at 1500°C and Partial Oxygen Pressure = 1.26 x 10^{-9} atm

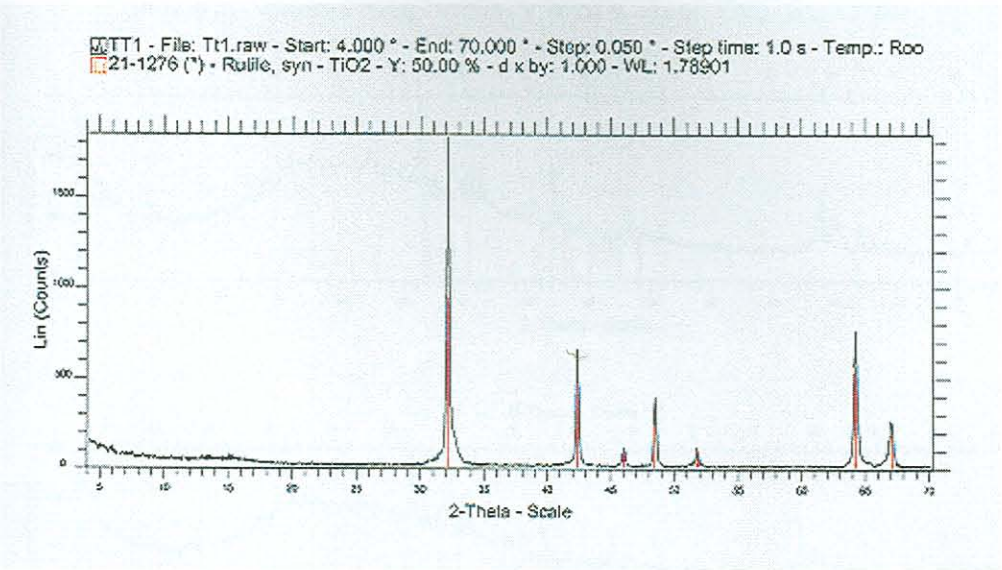

Fig. 4.7: EPMA(WDS) Analyses on 50T15 Sample

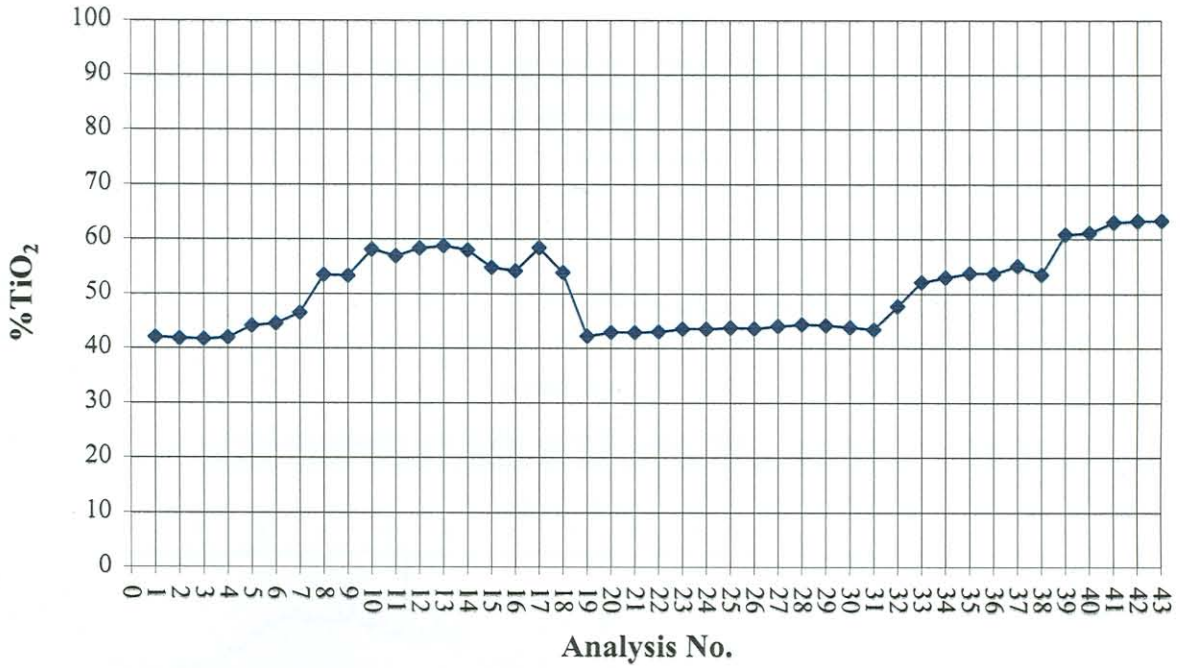

Fig. 4.8: XRD Analyses of 70 mass% TiO_2 Samples Compared with XRD Data for best fitting Magneli Phases

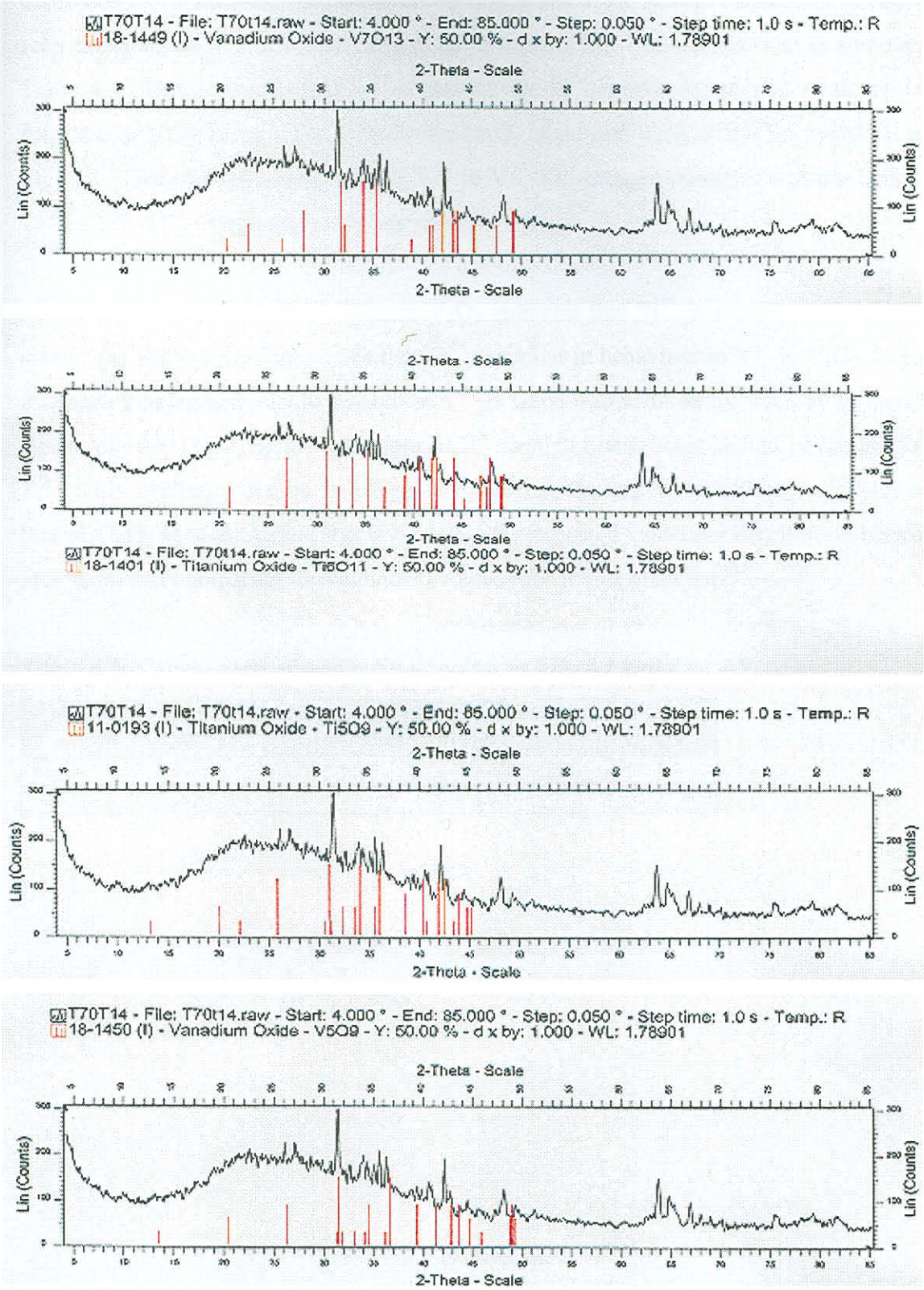

When the composition points for the M_3O_5 and M_4O_7 phases boundaries in Fig. 4.1 are compared to the composition points for the Ti_3O_5 and Ti_4O_7 phases boundaries in Fig. 4.9 it is seen these composition points correspond in magnitude. The comparison is summarised in Table 4.5. This indicates that V^{3+} substitute for Ti^{3+} within the crystal structure with the formulas actually being $V_2O_3.TiO_2$ for the M_3O_5 phase and $V_2O_3.2TiO_2$ for the M_4O_7 phase in Fig. 4.1. Therefore the behaviour of V^{3+} in V^{3+}-Ti^{4+}-oxygen mixtures and the behaviour of Ti^{3+} in Ti^{3+}-Ti^{4+}-oxygen mixtures are similar.

Furthermore the solubility of TiO_X in V_2O_3 indicates that Ti^{3+} is stabilised in the V_2O_3-rich side of the V_2O_3-TiO_2 diagram, or that Ti^{4+} is similar in behaviour to V^{4+} in V_2O_3. In Fig. 4.10 it is seen that an appreciable amount of V^{4+} is taken into solution by V_2O_3 at temperatures in excess of 1000 °C. Thus the behaviour of V^{3+} in high titania slags should be similar to that of Ti^{3+}. This similarity can be investigated by setting the activity coefficient of V_2O_3 equal to that of Ti_2O_3 in high titania slags to calculate the expected vanadium distribution between slag and metal and comparing the calculated values with actual plant data*.

Table 4.5: Comparison of composition points in Fig. 4.1 and Fig. 4.9

Phase Type	Mole Fraction Ti^{4+}: Fig. 4.9 (Ti_2O_3-TiO_2 system)	Mole Fraction Ti: Fig. 4.1 (V_2O_3-TiO_2 system)
M_3O_5	0.33	~ 0.40
M_4O_7	0.50	~ 0.55

*Private Communication: Dr. W.H. van Niekerk, Iscor Heavy Minerals

Fig. 4.9: Optimised Ti_2O_3-TiO_2 phase diagram: Eriksson and Pelton[12]

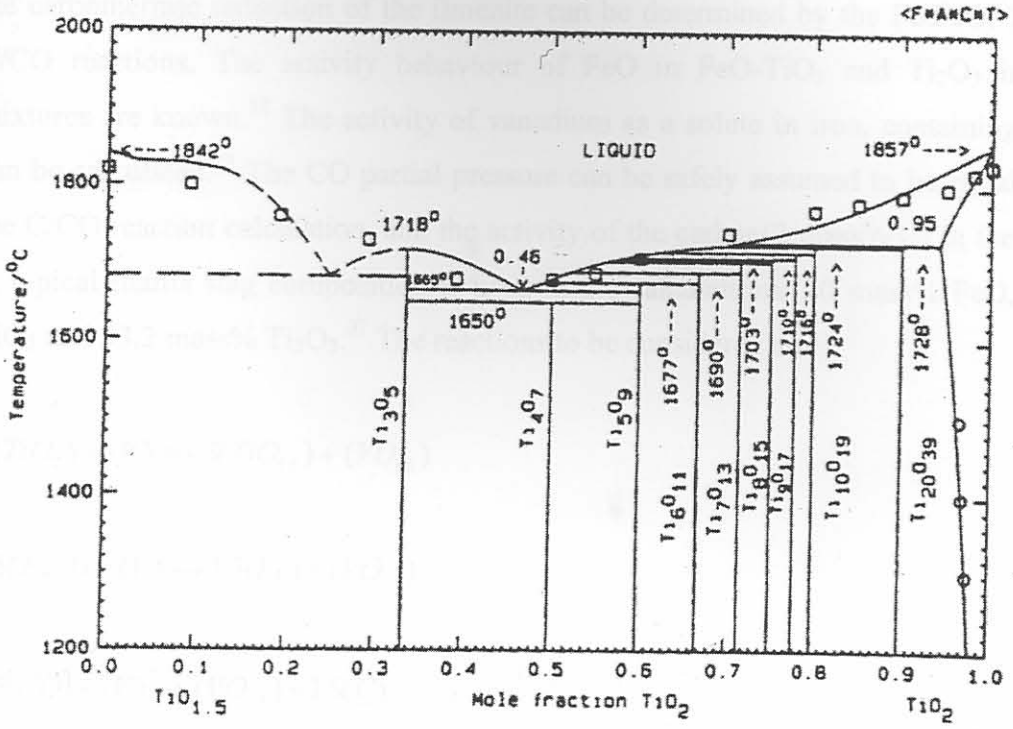

Fig. 4.10: V-O phase diagram: Wriedt[19]

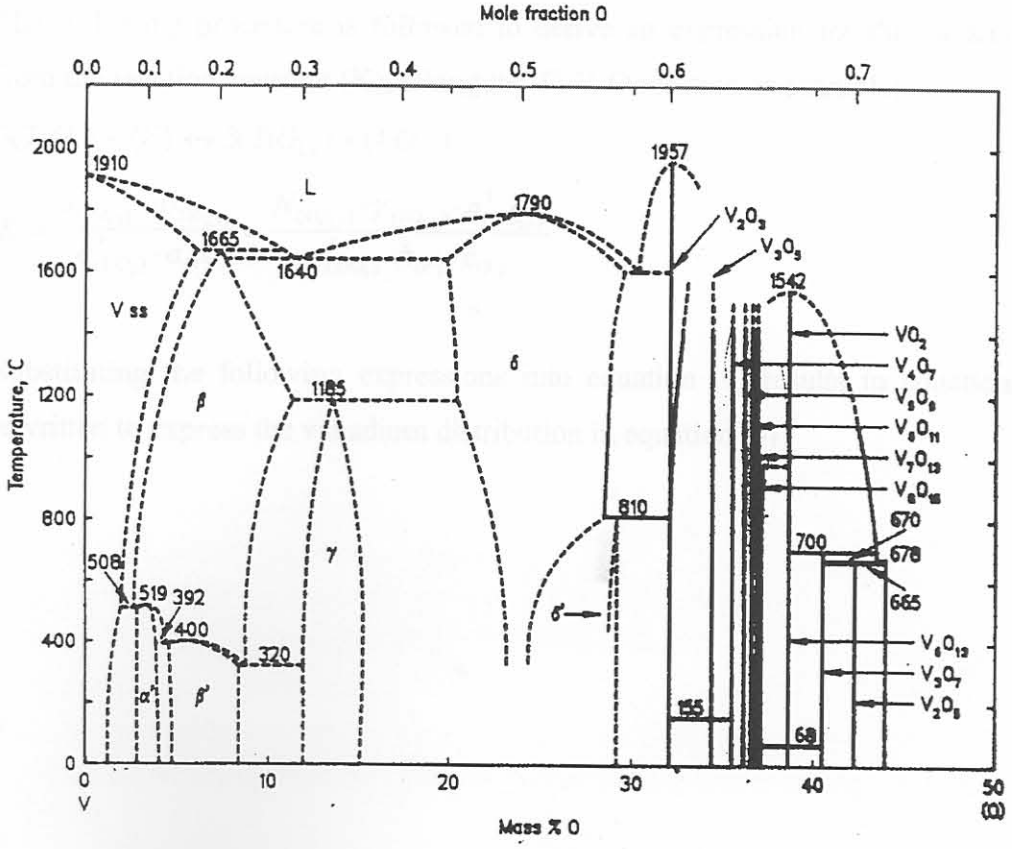

In calculating the vanadium distribution from thermodynamics the partial oxygen pressure in the carbothermic reduction of the ilmenite can be determined by the Fe/FeO, Ti_2O_3/TiO_2 or C/CO reactions. The activity behaviour of FeO in $FeO\text{-}TiO_2$ and Ti_2O_3 in $Ti_2O_3\text{-}TiO_2$ mixtures are known.[12] The activity of vanadium as a solute in iron, containing 2 mass% C, can be calculated.[33] The CO partial pressure can be safely assumed to be equal to 1 atm for the C/CO reaction calculation, and the activity of the carbon(2 mass% C) in the iron is 0.1.[39] A typical titania slag composition is used in the calculations: 10 mass% FeO, 51.8 mass% TiO_2 and 33.2 mass% Ti_2O_3.[37] The reactions to be considered are:

$$3(TiO_2) + \langle V \rangle \leftrightarrow 3(TiO_{1.5}) + (VO_{1.5}) \quad (1)$$

$$1.5(FeO) + \langle V \rangle \leftrightarrow 1.5(Fe) + (VO_{1.5}) \quad (2)$$

$$1.5[CO] + \langle V \rangle \leftrightarrow (VO_{1.5}) + 1.5(\underline{C}) \quad (3)$$

(X): Component X is in the liquid state

$\langle X \rangle$: Component X is in the solid state

$[X]$: Component X is in the gas phase

The following procedure is followed to derive an expression for the vanadium distribution from the reaction constant (K), taking the Ti-V-O reaction as example:

$$3(TiO_2) + \langle V \rangle \leftrightarrow 3(TiO_{1.5}) + (VO_{1.5}) \quad (1)$$

$$K = \frac{a_{(VO_{1.5})} \cdot a^3_{(TiO_{1.5})}}{a^3_{(TiO_2)} \cdot a_{\langle V \rangle}} = \frac{N_{(VO_{1.5})} \cdot \gamma_{(VO_{1.5})} \cdot a^3_{(TiO_{1.5})}}{a^3_{(TiO_2)} \cdot h_{\langle V \rangle} \cdot c_{\langle V \rangle}} \quad (4)$$

Substituting the following expressions into equation (4) results in equation (5), which is rewritten to express the vanadium distribution in equation (6).

$$h_{\langle V\rangle} = \langle \%V \rangle \cdot f_{\langle V\rangle}$$

$$\log(f_{\langle V\rangle}) = e_V^C \cdot (\%C)$$

$$c_{\langle V\rangle} = \frac{mm_{Fe} \cdot \gamma_V^\circ}{100 \cdot mm_V}$$

$$N_{(VO_{1.5})} = \frac{\%V_2O_3 \cdot mm_{slag}}{100 \cdot mm_{(VO_{1.5})}}$$

$$\%V_2O_5 = \frac{\%V_2O_3 \cdot mm_{V_2O_5}}{mm_{V_2O_3}} = 1.213(\%V_2O_3)$$

$mm_{slag} = 76.02 g/mol$ (average value)

$$K = \frac{0.836 \cdot (\%V_2O_5) \cdot \gamma_{(VO_{1.5})} \cdot a^3_{(TiO_{1.5})}}{100 \cdot a^3_{(TiO_2)} \cdot \langle \%V \rangle \cdot f_{\langle V\rangle} \cdot c_{\langle V\rangle}} \qquad (5)$$

$$\frac{(\%V_2O_5)}{\langle \%V \rangle} = L_V = \frac{100 \cdot K \cdot a^3_{(TiO_2)} \cdot f_{\langle V\rangle} \cdot c_{\langle V\rangle}}{0.824 \cdot \gamma_{(VO_{1.5})} \cdot a^3_{(TiO_{1.5})}} \qquad (6)$$

Similar expressions for the vanadium distribution can be developed for reactions (2) and (3) by following the same procedure as set out here for reaction (1).

---

a_i = activity of component i

N_i = mole fraction of component i

γ_i = Raoultian activity coefficient of component i

f_i = Henrian activity coefficient of component i with the 1 mass% solution as the reference state

e_V^C = first order interaction coefficient of C on V in liquid iron

mm_i = molar mass of component i

γ_V° = activity coefficient of vanadium at infinite dilution in liquid iron

h_i = Henrian activity coefficient of i with pure i as the reference state

The calculated vanadium distribution values and the vanadium distribution values obtained from plant data are shown in Fig. 4.11. It is seen that the plant vanadium distributions are independent of temperature and that the plant values are larger than that calculated from the C/CO and Fe/FeO reactions, but slightly below the values calculated for the Ti_2O_3/TiO_2, indicating that the reduction of vanadium from the slag into the metal, from a system oxygen partial pressure point of view, is likely to be controlled by an interaction between reaction (1) and reaction (2).

Fig. 4.11: Vanadium Distribution: Calculated vs. Actual

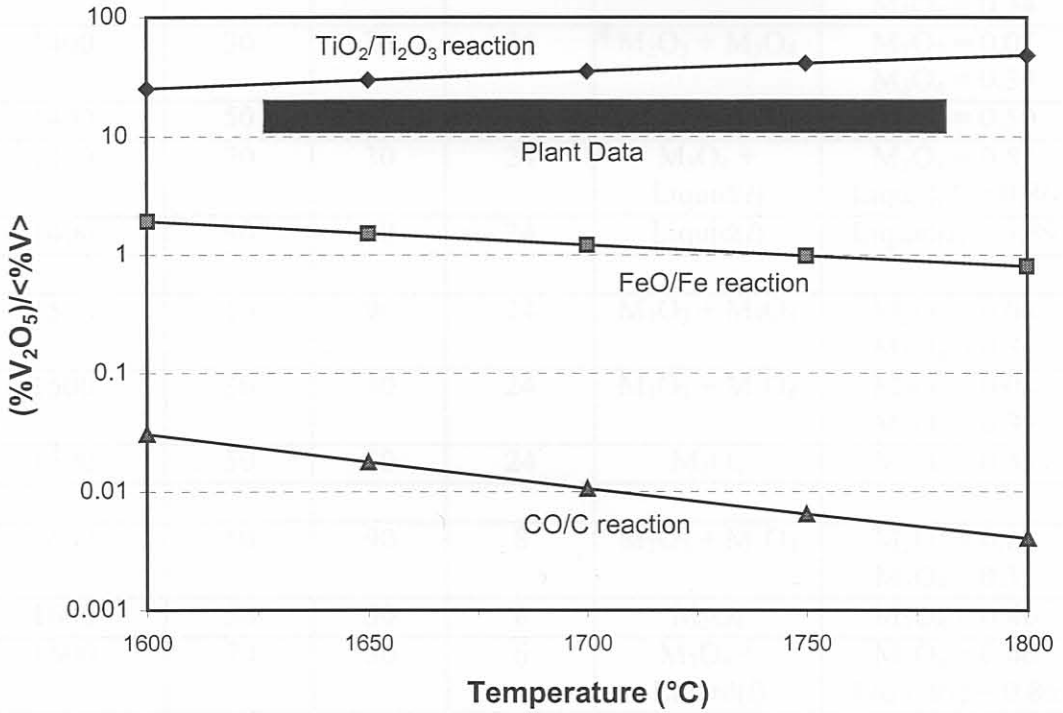

The conclusion made from the work discussed in this section is that vanadium and titanium cations, V^{3+} and Ti^{3+}, and V^{4+} and Ti^{4+} substitute for each other in oxide solid solutions under the conditions of partial oxygen pressure and temperature used in this work. Furthermore, the chemical behaviour of V_2O_3 in high titania slags is similar to that of Ti_2O_3 in these slags. This knowledge made the thermodynamic calculation of the vanadium distribution within these slags possible, indicating that the vanadium distribution is most likely controlled by an interaction between reaction (1), the TiO_2/Ti_2O_3 reaction, and reaction (2), the FeO/Fe reaction.

4.2. V_2O_3 - FeO System

Table 4.6 gives a summary of the sample compositions reacted, the reaction times used and phases identified in each sample. The reacted samples were subjected to XRD analysis, optical microscopy under reflected light and EPMA with an EDS facility.

Table 4.6: Summary of Experiments

Reaction Temperature (°C)	Initial Composition (Mass %)		Reaction Time (Hours)	Phases Identified	mol Fe/ (mol Fe +mol V) in Phase
	Fe_2O_3	V_2O_5			
1400	10	90	24	$M_2O_3 + M_3O_4$	$M_2O_3 = 0.07$ $M_3O_4 = 0.34$
1400	30	70	24	$M_2O_3 + M_3O_4$	$M_2O_3 = 0.07$ $M_3O_4 = 0.34$
1400	50	50	24	M_3O_4	$M_3O_4 = 0.50$
1400	70	30	24	M_3O_4 + Liquid(l)	$M_3O_4 = 0.57$ Liquid(l) = 0.86
1400	90	10	24	Liquid(l)	Liquid(l) = 0.89
1500	10	90	24	$M_2O_3 + M_3O_4$	$M_2O_3 = 0.08$ $M_3O_4 = 0.34$
1500	30	70	24	$M_2O_3 + M_3O_4$	$M_2O_3 = 0.08$ $M_3O_4 = 0.35$
1500	50	50	24	M_3O_4	$M_3O_4 = 0.45$
1600	10	90	8	$M_2O_3 + M_3O_4$	$M_2O_3 = 0.08$ $M_3O_4 = 0.35$
1600	50	50	8	M_3O_4	$M_3O_4 = 0.40$
1600	70	30	6	M_3O_4 + Liquid(l)	$M_3O_4 = 0.46$ Liquid(l) = 0.86

The phase diagram deduced from the information in Table 4.6 is shown in Fig. 4.12. The diagram consists of five phase fields in which three different phases, i.e. M_2O_3, M_3O_4 and liquid could be distinguished, where M indicates both vanadium and iron ions. The M_2O_3 and M_3O_4 phases were both solid at all of the experimental temperatures.

The XRD patterns for the series of samples reacted at 1400°C are shown in Fig. 4.13. The corresponding photomicrographs for the samples are shown in Fig. 4.14. A summary of the EPMA analyses is shown in Appendix 5.

The samples of 10 and 30 mass% Fe_2O_3 initial composition contained the two solid-solutions of M_2O_3 and M_3O_4. These phases appeared as a banded structure within each other as is shown in Fig. 4.14. The samples of 50 mass% Fe_2O_3 initial composition consist of the spinel

solid-solution(M_3O_4) only, and therefore have to lie within the spinel phase field. Because only one phase was present within these samples their chemical composition should be close to the initial composition, as is the case for the sample reacted at 1400°C. However, the samples for 1500°C and 1600°C shifted in composition from the 0.53 mole fraction Fe composition, to compositions containing less iron, as is shown in Table 4.7. A possible explanation for this is the absorption of iron into the platinum wire sample containers, with an increase in the quantity of iron diffusing into the Pt and Pr-Rh wire, with an increase in experimental temperature. This does not influence the position of the phase boundaries of the spinel solid-solution phase field because samples consisting of only one phase as is the case for the 50 mass% Fe_2O_3-50 mass% V_2O_5 initial sample compositions, is not used in plotting phase boundaries. The 70 mass% Fe_2O_3 sample reacted at 1400°C consisted of liquid and spinel solid-solution as shown in Fig. 4.14 and indicated the phase boundaries for liquid and the M_3O_4 phase at 1400°C. The presence of liquid in this sample is affirmed by the presence of quench crystals, which are fine dot-like crystals, that crystallised from the liquid on quenching the sample. The sample of 70 mass% Fe_2O_3 reacted at 1600°C was reacted for six hours instead of the required equilibrium time of eight hours. This shortened reaction period was used because with increasing temperatures, above 1400°C, more liquid formed. The liquid dripped from the Pt-Rh wire cone more easily, perforating the PVC layer which closed off the furnace tube, so rendering the experiment useless. The standard deviation in the EPMA analyses for the mol Fe, shown in Appendix 5, is 0.004 for the M_3O_4 phase and 0.052 for the liquid phase. This can be compared for the standard deviation, on the mol Fe, for the sample of 70 mass% Fe_2O_3 reacted for 24 hours at 1400°C: 0.006 for the M_3O_4 phase and 0.005 for the liquid phase. Because the standard deviations on the EPMA analyses are comparable for the samples reacted for 24 and 6 hours respectively, the data generated from the 6 hour sample is used to plot the phase diagram.

Table 4.7: Composition Differences for 50 mass% Fe_2O_3 - 50 mass% V_2O_5 Initial Sample Composition

Particular Sample	Mol V	mol Fe	Mole fraction Fe
Theoretical Input Into Sample	0.55	0.63	0.53
1400°C Sample	0.68	0.69	0.50
1500°C Sample	0.75	0.61	0.45
1600°C Sample	0.81	0.55	0.40

Fig. 4.12: V_2O_3 - FeO Phase Diagram

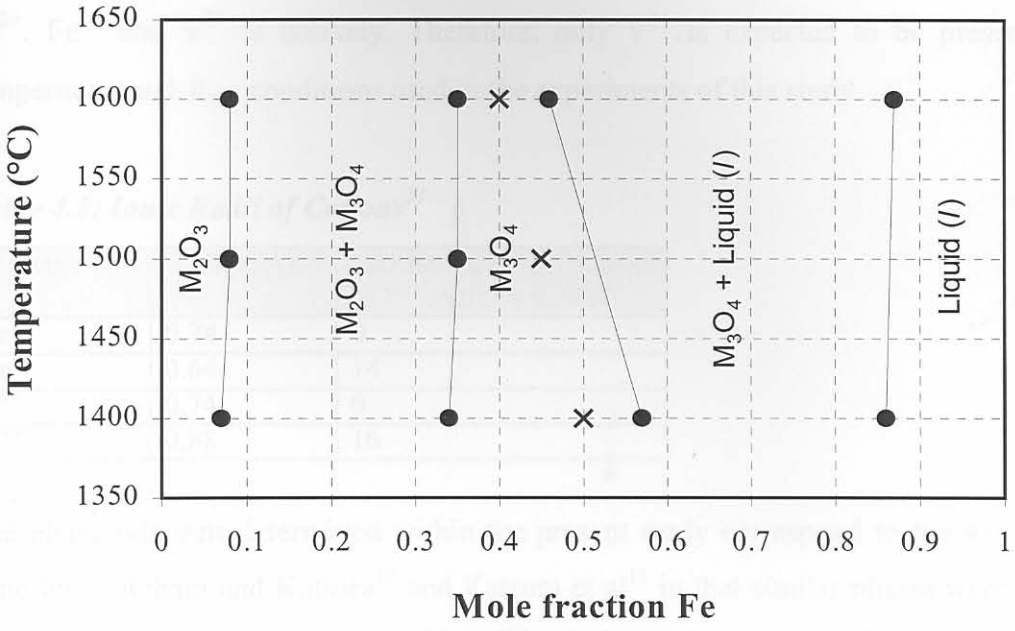

× : Composition points of samples consisting of one phase

• : Composition points of respective phases in two phase samples

The 90 mass% Fe_2O_3 sample reacted at 1400°C consisted of liquid only as indicated by the absence of any crystals in the photomicrograph shown in Fig. 4.14. The absence of crystals was also observed under the electron microscope at large magnifications. Another important indication that this sample was molten at the experimental temperature is that the sample formed individual droplets on quenching and the remainder of the liquid wetted the Pt-Rh wire container. The XRD pattern of this sample is shown in Fig. 4.13 and it indicates that the sample consisted of wüstite and a small quantity of magnetite, once the sample had solidified. The magnetite formed on quenching, when wüstite transformed to magnetite.[23] The transformation could however not be completed because of quenching of the sample, halting the transformation reaction at an early stage. The existence of 100% liquid in the 90 mass% Fe_2O_3 - 10 mass% V_2O_5 sample, at 1400°C, can be compared to the liquidus temperature of wüstite at $P_{O_2} = 1 \times 10^{-9.5}$ atm of 1377°C.[23]

From the co-ordination of cations to oxygen as indicated by the XRD analyses M^{2+} and M^{3+} cations are expected in the solid and liquid solutions formed in the FeO-V_2O_3 system. When the ionic radii of Fe^{2+}, Fe^{3+}, V^{2+} and V^{3+} are compared, see Table 4.8, it is seen that substitutional solid solution formation between Fe^{2+}, Fe^{3+} and V^{3+} is likely to occur because

the ionic radii of these cations differs by less than 15%. The ionic radius of V^{2+} differs from those of Fe^{2+} and Fe^{3+} by more than 15%, indicating that solid-solution formation between Fe^{2+}, Fe^{3+} and V^{2+} is unlikely. Therefore, only V^{3+} is expected to be present under the temperature and P_{O_2} conditions used in the experiments of this study.

Table 4.8: Ionic Radii of Cations[24]

Cation	Radius (Å)	%Difference with respect to V^{3+} radius = 0.74 Å
Fe^{2+}	0.74	0
Fe^{3+}	0.64	14
V^{3+}	0.74	0
V^{2+}	0.88	16

The phase relations determined within the present study correspond to the work previously done by Wakihara and Katsura[10] and Katsura et al[11] in that similar phases were identified in the present study, that is a sesquioxide solid solution and a spinel solid solution.

Fig. 4.13: XRD Patterns for Fe_2O_3 - V_2O_5 Samples reacted at 1400°C

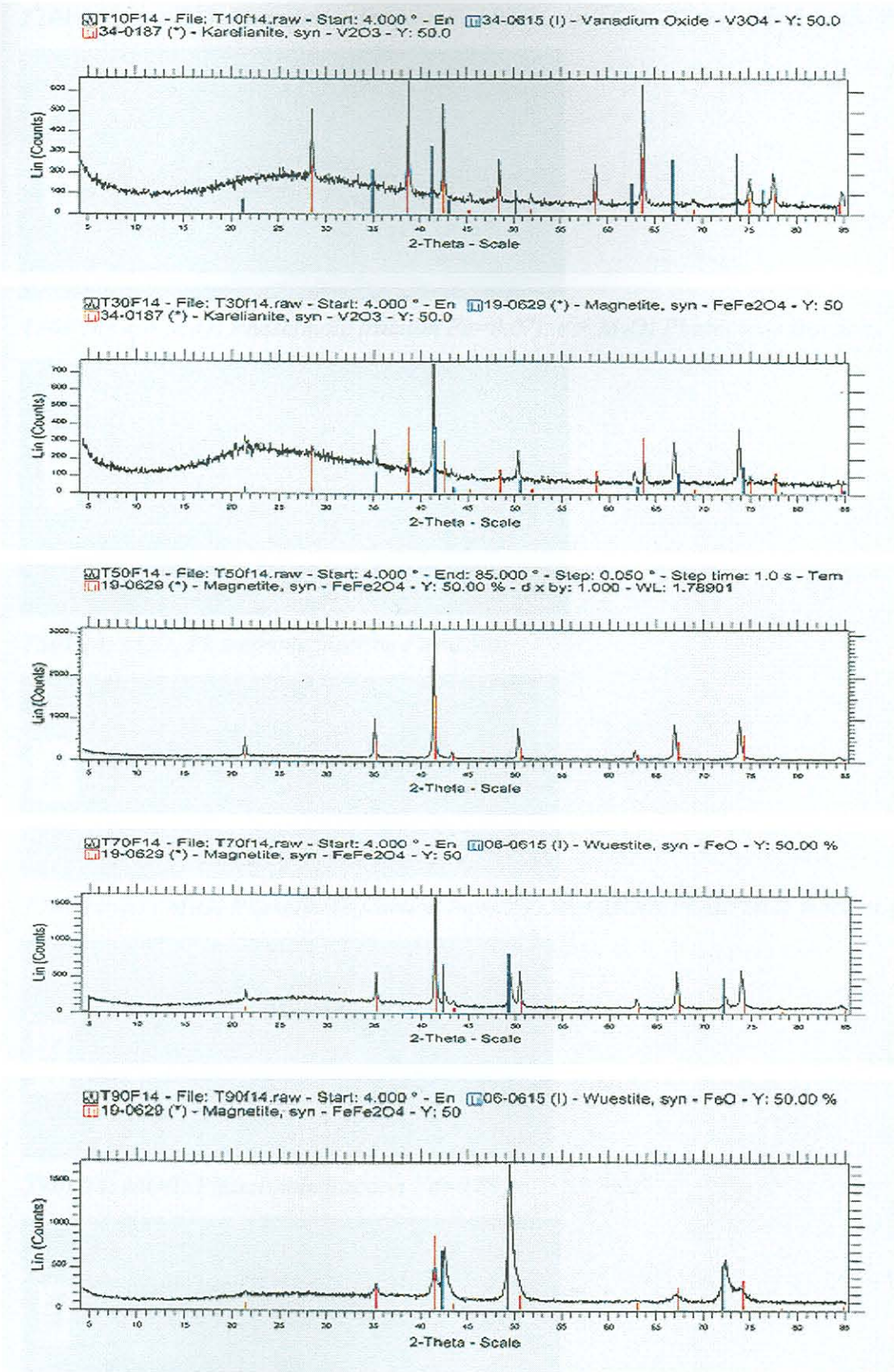

T10F14 = 10 mass% Fe_2O_3 in initial sample; T30F14 = 30 mass% Fe_2O_3 in initial sample;

T50F14 = 50 mass% Fe_2O_3 in initial sample; T70F14 = 70 mass% Fe_2O_3 in initial sample;

T90F14 = 90 mass% Fe_2O_3 in initial sample

Fig. 4.14: Photomicrographs for Fe_2O_3 - V_2O_5 Samples reacted at 1400°C

T10F14: *a = M_2O_3 Phase(mole fraction Fe=0.07), e = M_3O_4 Phase(mole fraction Fe=0.34)*

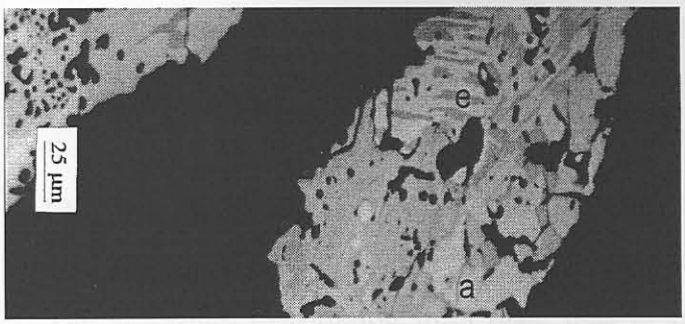

T30F14: *a = M_2O_3 Phase(mole fraction Fe=0.07), e = M_3O_4 Phase(mole fraction Fe=0.34)*

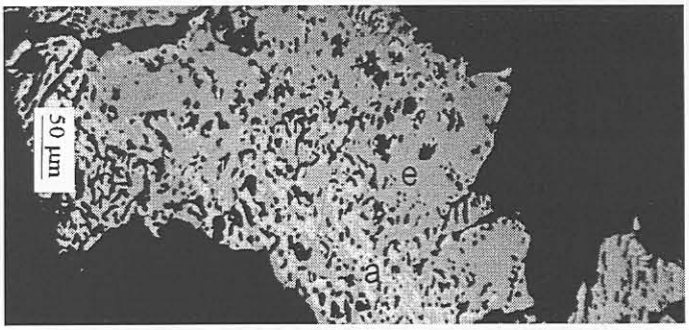

T50F14: *M_3O_4 Phase(mole fraction Fe=0.50)*

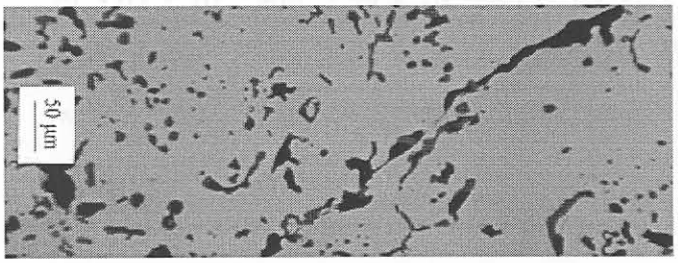

T70F14: *a = M_3O_4 Phase(mole fraction Fe=0.57), c = MO(l) Phase(mole fraction Fe=0.86)*

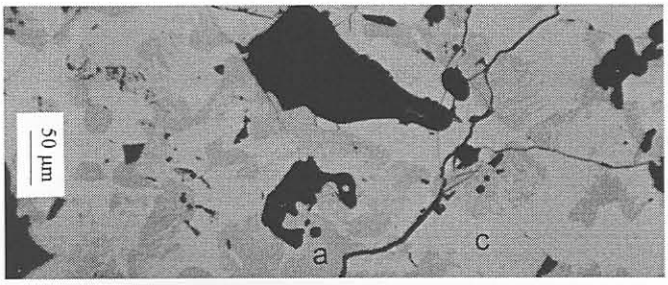

T90F14: *MO(l) Phase(mole fraction Fe=0.89)*

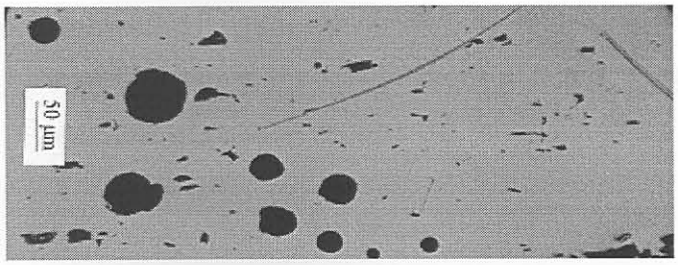

T10F14 = 10 mass% Fe_2O_3 in initial sample; T30F14 = 30 mass% Fe_2O_3 in initial sample;

T50F14 = 50 mass% Fe_2O_3 in initial sample; T70F14 = 70 mass% Fe_2O_3 in initial sample;

T90F14 = 90 mass% Fe_2O_3 in initial sample

5. CONCLUSIONS

- The V_2O_3-TiO_2 pseudo-binary phase diagram consists of the solid solution phases M_2O_3, M_3O_5 and higher Magneli phases, M=(V, Ti), in equilibrium with a gas mixture of CO and CO_2 of volumetric ratio of 3 representing partial oxygen pressures of 3.02×10^{-10} atm, 2.99×10^{-9} atm and 2.31×10^{-8} atm at 1400°C, 1500°C and 1600°C respectively. In the Ti-V oxide solid solutions V^{3+} and Ti^{3+} substitute for each other, and V^{4+} and Ti^{4+} substitute for each other. Furthermore, the chemical behaviour of V_2O_3 in TiO_2 is similar to that of Ti_2O_3. The vanadium distribution from plant data is situated between the calculated vanadium distributions for the Fe/FeO reaction and the Ti_2O_3/TiO_2 reaction, indicating that the vanadium distribution is likely to be controlled, in terms of partial oxygen pressure, by interaction between these two reactions.

- The V_2O_3-FeO pseudo-binary phase diagram consists of the phases M_2O_3, M_3O_4 and liquid, M=(V, Fe), in the temperature range of 1400°C-1600°C and in equilibrium with a gas mixture of CO and CO_2 of volumetric ratio of 3 representing partial oxygen pressures of 3.02×10^{-10} atm, 2.99×10^{-9} atm and 2.31×10^{-8} atm at 1400°C, 1500°C and 1600°C respectively. From ionic radius calculations V^{3+}, Fe^{3+} and Fe^{2+} substitute for each other within the M_2O_3 and M_3O_4 solid solution phases

- The experimental technique used in this study is suitable for phase relation determinations within the pseudo-binary systems FeO-V_2O_3 and TiO_2-V_2O_3 in the temperature range of 1400°C-1600°C and at partial oxygen pressures of 3.02×10^{-10} atm. to 2.31×10^{-8} atm., and should be suitable for phase relation studies in the pseudo-ternary system TiO_2-V_2O_3-FeO under the same conditions of temperature and partial oxygen pressure.

- The data gathered in this study provides a starting point from which phase relations in the pseudo-ternary system TiO_2-V_2O_3-FeO can be determined. Furthermore, this data confirms that high melting components exist within the TiO_2-rich region of the system so that future investigations into phase relations within this region of the system should be conducted at temperatures above 1600°C.

6. RECOMMENDATIONS FOR FUTURE WORK

- Phase relations in the pseudo-ternary system TiO_2-FeO-V_2O_3 should be determined at temperatures of at least 1600°C in order to identify the liquid phase field within the system.

- Subsequently, activity-composition relations of iron oxides and vanadium oxides in the TiO_2-rich liquid phase area of the TiO_2-FeO-V_2O_3 pseudo-ternary should be determined.

- The experimental procedure used in the present study can serve as the basis of the approach to be followed in doing the proposed future work.